

A 40Gb/s PAM4 Transmitter based on a Ring-resonator Optical DAC

*Sajjad Moazeni
Vladimir Stojanovic*

Electrical Engineering and Computer Sciences
University of California at Berkeley

Technical Report No. UCB/EECS-2017-23

<http://www2.eecs.berkeley.edu/Pubs/TechRpts/2017/EECS-2017-23.html>

May 1, 2017



Copyright © 2017, by the author(s).
All rights reserved.

Permission to make digital or hard copies of all or part of this work for personal or classroom use is granted without fee provided that copies are not made or distributed for profit or commercial advantage and that copies bear this notice and the full citation on the first page. To copy otherwise, to republish, to post on servers or to redistribute to lists, requires prior specific permission.

Acknowledgement

The author would like to thank Prof. Milos A. Popovic, Mark T. Wade, Sen Lin, Taehwan Kim, Nandish Mehta, Pavan Bhargava and the Berkeley Wireless Research Center (BWRC) staff. This work was supported in part by DARPA POEM award HR0011-11-C-0100, NSF ECCS award 1611296 and the BWRC. The views expressed are those of the author and do not reflect the official policy or position of the DoD or the US Government.

A 40Gb/s PAM4 Transmitter based on a Ring-resonator Optical
DAC

by Sajjad Moazeni

Research Project

Submitted to the Department of Electrical Engineering and Computer Sciences, University of California at Berkeley, in partial satisfaction of the requirements for the degree of **Master of Science, Plan II**.

Approval for the Report and Comprehensive Examination:

Committee:



Professor Vladimir Stojanović
Research Advisor

12/12/2016

Date

* * * * *



Professor Elad Alon
Second Reader

12-14-16

Date

Contents

1	Introduction	1
2	Background	3
2.1	Silicon Photonics Interconnects	4
2.1.1	Microring Resonators	4
2.1.2	Optical Link Anatomy	5
2.2	Silicon Photonics Platforms	8
2.2.1	Heterogeneous vs. Monolithic Integration	8
2.2.2	Silicon Photonics in Zero-change SOI CMOS Process	9
3	Ring-resonator based Optical DAC	11
3.1	Spoked-ring Resonators	11
3.2	Optical DAC (ODAC)	12
4	PAM4 Optical Transmitter	15
4.1	Prior PAM4 Optical Transmitters	15
4.2	Ring-resonator Thermal Tuning	16
4.3	High-Speed Digital PLL	17
4.4	ODAC based PAM4 Transmitter	17
5	Measurement Results	20
6	Conclusion	24

List of Figures

2.1	Ring-resonator characteristics and transfer function.	5
2.2	Anatomy of ring-resonator based optical links [8].	6
2.3	Optical WDM links [8].	7
2.4	Hetrogeneous integrations of photonics [12].	8
2.5	Cross-section of 45nm 12SOI CMOS process [9].	10
3.1	Spoked-ring modulator: (a) 3D rendering of layout; (b) FDTD simulation; (c) PN junctions mask; (d) Micrograph [20].	11
3.2	Optical DAC concept.	12
3.3	Linearity comparison of the proposed optical DAC vs. electrical DAC driven ring-resonator.	14
4.1	PAM4 optical transmitter architectures: (a) Segmented MZI with electrical DAC [3]; (b) Ring-modulator driven by an electrical DAC [21].	16
4.2	Thermal effects on ring-modulators.	17
4.3	20GHz Digital PLL block-digram.	18
4.4	PAM4 transmitter block-diagram.	19
4.5	Chip micro-graphs.	19
5.1	Flipchip packaging.	21
5.2	Test setup.	21
5.3	Static optical DAC measurements.	22
5.4	Transmit eye-diagrams.	22
5.5	Transmitter area and energy breakdown.	23
6.1	Comparison and performance summary table.	25

Abstract

Next generations of large data-centers and supercomputers are lagging due to the stagnation of interconnects speed. Silicon-photonics has been proposed as a potential solution to achieve low-cost, high-speed, and energy-efficient optical links in silicon-based processes. This work presents an optical digital-to-analog converter based on a segmented, active microring resonator in a zero-change commercial 45nm SOI CMOS process. Using this design approach, a monolithically integrated 40Gb/s PAM4 transmitter is demonstrated with 42fJ/b modulator and driver energy and 0.67Tb/s/mm² bandwidth density. This scheme is suitable for systems-on-chips with large number of I/O links such as processors and switches in large-scale computing and storage systems.

Chapter 1

Introduction

Silicon photonics is a promising technology to realize low cost and energy-efficient optical links for emerging large-scale rack-to-rack and within-rack data-center applications, and general purpose supercomputer interconnect. The performance metrics in these applications require highly integrated electronic-photonics circuits. Various integration strategies have been utilized to implement high performance electro-optical systems including hybrid, heterogeneous and monolithic integration. Among these, monolithic integration has the potential for reliable, low-cost and large-scale integration, while being most promising in terms of energy-efficiency and bandwidth-density of implemented photonic links. Recently, the possibility of implementing ultra power-efficient silicon photonic links using an unmodified (zero-change) state-of-the-art 45nm SOI CMOS process has been demonstrated. This approach enabled the fabrication of millions of transistors and hundreds of photonic devices in the same chip to improve processor-memory link bandwidth, and opened a path to solving this traditional computation bottleneck [1].

In this work, we demonstrate the capability of implementing high-speed optical transmitters meeting the needs of data centers for 100G/400G Ethernet in the same platform, with ultra-low power consumption, by using a higher order Pulse Amplitude Modulation (PAM) technique. PAM4 modulation has been recently adopted in optical transceivers to accommodate the emerging PAM4 electrical line rates and modulation formats without the need to introduce the PAM4 to NRZ gearshift boxes. Multi-level optical intensity can be

generated by the use of an electrical digital-to-analog converter (DAC) driving an optical Mach-Zehnder interferometer (MZI) modulator and/or segmenting the phase-shift portions of the MZI (optical phase DAC) and driving them digitally. Using a purely optical DAC eliminates the extra non-linearity, power consumption and area overhead of the electrical DAC. Optical-DAC based MZI modulators have been demonstrated in [2, 3]. However, MZIs with high-enough extinction ratio (ER) are inherently millimeter-sized devices, which leads to high energy consumption, high insertion loss (IL), and large footprints.

We demonstrate an optical DAC based on a segmented ring-resonator modulator. Measurements show two orders of magnitude improvement in energy efficiency compared to MZI-based optical DACs. Moreover, micro-ring modulators have tens-of-microns footprint and support wavelength division multiplexing (WDM) that enables large-scale, high-bandwidth density integrated systems (with bandwidth densities in the $Tb/s/mm^2$).

Chapter 2

Background

Fiber optics has been utilized historically in transatlantic communications for the first time [4]. Since then, the optical communication is known as the solution for long distance and high-data rate applications. As the bandwidth requirements continue to scale due to the drastic increase of Internet traffic in data centers and also the demand for high performance computers, shorter and shorter distance links need to shift from copper to fiber optics. Today data-centers are upgrading their interconnect to support $25G$ for inter-rack and $100G$ for intra-rack communications, while projections for the near future are $50G$ and $200/400G$ respectively [5], which indicates a huge gap that can be filled by exploiting optical links.

As optical links are getting more popular, finding a scalable solution that addresses all the communication needs is a big challenge. Silicon photonics is the most promising technology for this aim. The key advantage of using CMOS technology to build optical transceivers is the lower-cost and higher yield than other platforms; Moreover advanced lithographic processes helps to design precise structures for photonic devices that are in close proximity to integrated circuits with small interconnect parasitics.

We will review the basics of ring-resonator based optical links and their benefit over other approaches in Section 2.1. Section 2.2, outlines different electro-optical platforms and introduces our zero-change CMOS silicon photonics technology.

2.1 Silicon Photonics Interconnects

2.1.1 Microring Resonators

The micro-ring resonator is a ring shaped waveguide that can trap the input light from the bus waveguide coupled into it. In other words, whenever the circumference of the ring is an integer multiple of the input light wavelength, namely λ_0 , the coupled light wave from the bus port will interfere constructively in the ring cavity by traveling through the ring circumference and building up the optical power. Consequently, through-port intensity will be reduced significantly. This behavior can be translated as a set of notches in the wavelength domain, shown in Figure 2.1.

Resonance spacings are called free spectral range (FSR) and rings with smaller radius have larger FSR. Since any multiple wavelengths can satisfy constructive interference condition, FSR can be quantitatively derived:

$$\lambda_0 = \frac{n_{eff}L}{m}, m = 1, 2, 3, \dots \quad (2.1)$$

$$FSR = \frac{\lambda^2}{n_g L} \quad (2.2)$$

Where L is the circumference of the ring, and n_g is the group index, which takes the dispersion of the silicon waveguide into account. In multi wavelength communication systems such as WDM links, all the channels should fit in one FSR and generally larger FSRs are preferable for modulators in optical communications.

Through-port transfer function can be derived as a function of cross-coupling coefficients between the bus waveguide and ring cavity and also the round trip loss along the ring [6], as follows:

$$\alpha = \frac{I_{through}}{I_{input}} = \frac{\tau^2 - 2r\tau\cos\phi + r^2}{1 - 2r\tau\cos\phi + r^2\tau^2} \quad (2.3)$$

where $\phi = (2\pi n_{eff}/\lambda)L$ ($\phi = 0$ when ring is on resonance) and τ is the total round trip loss (including drop-port coupling loss). This function can be simplified in terms of main

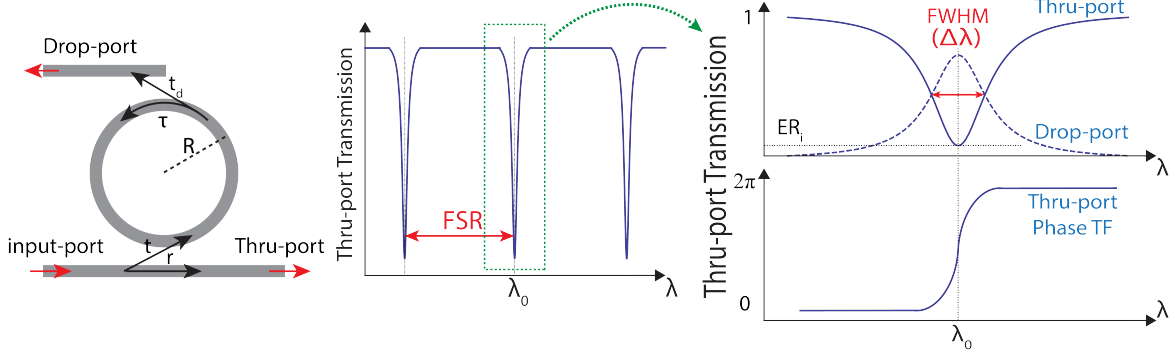


Figure 2.1: Ring-resonator characteristics and transfer function.

resonator parameters:

$$\alpha(\lambda) = 1 - \frac{A}{1 + 4\left(\frac{\lambda - \lambda_0}{\Delta\lambda}\right)^2} \quad (2.4)$$

where A represents the depth of the notch and $\Delta\lambda$ is microrings full-width half-maximum (FWHM) bandwidth, which is indicative of the sharpness of the resonance notch. Intrinsic extinction ratio (ER_i) is defined as the through-port transmission (from unity) when the ring is on resonance and it is equal to $ER_i = -10\log_{10}(1 - A)$. When the ring is critically coupled, $A = 1$ and ER_i is ideally infinite.

Another useful parameter is the quality factor (Q-factor) of the resonance that is defined as the ratio of the resonance wavelength to its bandwidth ($Q = \frac{\lambda_0}{\Delta\lambda}$).

2.1.2 Optical Link Anatomy

Optical links can be realized by modulating a microring resonator's resonance wavelength. This approach can be interpreted as the on-off keying (OOK) modulation of the input light in the frequency domain if the input laser wavelength is in the proximity of the resonance. One way to modulate the resonance of these resonators is to use electro-optical properties of the ring material to change the refractive index. Silicon is a popular material used to fabricate these structures and we know that it has a symmetric crystal, which makes silicon's optical

properties invariant to any applied electric field. However, it's been shown that changes in free carrier concentration causes linear change in the index of refraction [7]. Hence, we can form active cavities by injecting or depleting carriers inside the cavity. PN junctions are the common means for this purpose as the depletion region width can be controlled by the bias voltage.

Figure 2.2 shows how ring resonators can be used on both transmitter and receiver sides. At the transmit side, modulator switches between two resonances imprinting data stream on the through-port optical intensity. Extinction ratio (ER) can be defined as the ratio of the transmitted optical intensity between two states. Notice, there's a certain insertion loss (IL) even for the high-intensity state due to the limited amount of resonance shift imposed by the doping level and shape of PN junctions. IL and ER can be expressed in terms of the Q-factor, ER_i , and the amount of resonance shift per applied voltage. Speed of modulation is limited by the PN junctions dynamic characteristics in addition to the $\Delta\lambda$ which should accommodate the modulated signal bandwidth.

The wavelength selectivity characteristic of the ring resonators can help the receive side to bandpass filter the transmit signal. The selected portion of spectrum will be converted to the electrical signal by a photo diode (PD) and eventually trans-impedance amplifiers and samplers are used to recover the transmitted digital data.

Conventional optical transmitters use Mach-Zehnder interferometer (MZI)-based modulators, which are millimeter sized devices because of traveling wave mechanism behind their

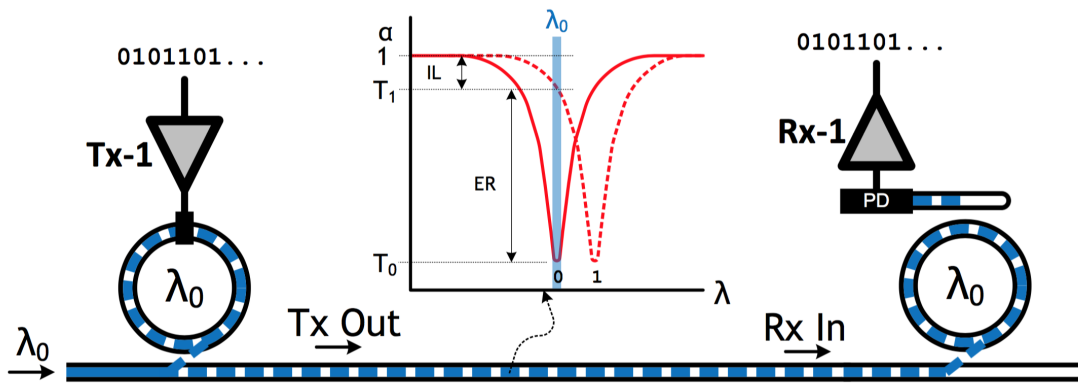


Figure 2.2: Anatomy of ring-resonator based optical links [8].

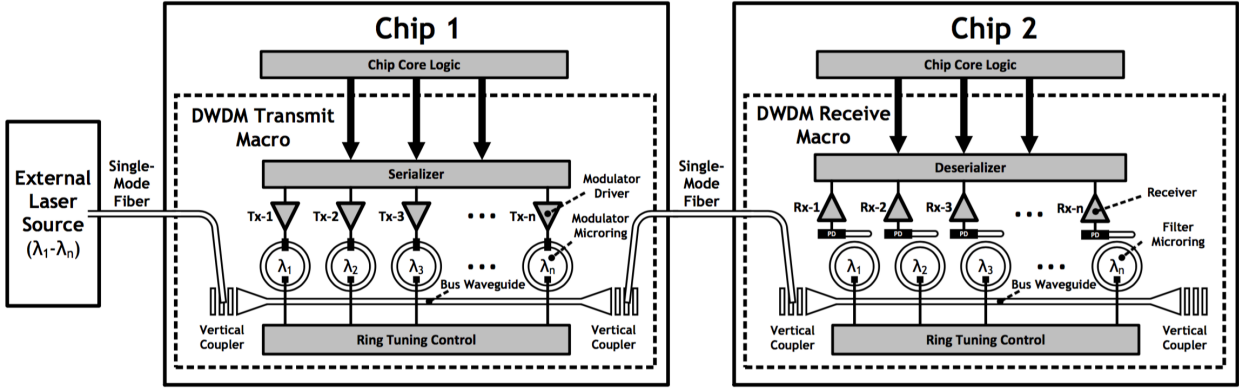


Figure 2.3: Optical WDM links [8].

physics. Large footprints make them energy inefficient, RC-bandwidth limited, and costly.

Main benefit of microring based optical links is the capability of communicating over multiple wavelengths simply by cascading them on transmitter and receiver side (Figure 2.3). This scheme is called wavelength division multiplexing (WDM), which is gaining popularity recently since it can improve aggregate link data-rates in a single fiber drastically. Absence of wavelength selectivity in MZIs makes them unfavorable in WDM systems as they need extra optical Mux/DeMux devices such as arrayed waveguide gratings (AWG). These multiplexers not only require milliliter size area, but also consumes relatively large static power for thermal tuning, while thermal tuning of ring resonators can be done in a very power efficient way [9].

It's worth noting that the cost of fiber and laser modules and also extra power and packaging issues added by extra lasers are preventing us from increasing total number of channels in WDM systems [10]. Recently many solutions such as laser combs [11] has been proposed to provide as many laser lines as possible, however they still provide limited number of channels. Thus, it's preferred to achieve higher data-rate per channel to minimize the energy consumption and cost of WDM links.

2.2 Silicon Photonics Platforms

2.2.1 Heterogeneous vs. Monolithic Integration

Silicon photonics integration is still a challenging problem as none of the proposed methods could address all the needs such as reliability, cost, low parasitics, etc so far. These approaches can be generally categorized in two subsets; Heterogeneous, where CMOS and photonics are fabricated on different wafers and attached afterwards [12, 13] by the use of TSV, copper pillars, etc. Since they can be separately optimized depending on their functionalities, this approach provides us with the flexibility to enhance the design space. However, the overhead of bonding process can be problematic from the aspect of yield, cost and extra interconnect parasitics.

An example of wafer-level heterogeneous 3D integration of silicon photonics is shown in Figure 2.4, where photonics SOI wafer is flipped on top of CMOS wafer and optical devices and circuits are connected using through-oxide-vias (TOVs) [12]. This method achieves relatively dense interconnects ($\sim 5\mu\text{m}$ pitch) with small parasitics of around $3fF$ per TOV.

Monolithic integration has emerged to address cost and fabrication issues of 3D integration and hybrid methods which also reduces interconnect parasitics by accommodating both optics and CMOS in a single wafer [1]. This method provides the smallest possible parasitics which is essential for building high-speed and energy-efficient optical links with

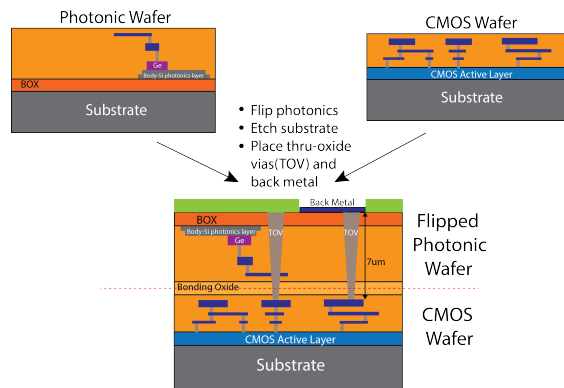


Figure 2.4: Heterogeneous integrations of photonics [12].

lower cost and higher yield than above-mentioned platforms. However, major downside is that a single fabrication process should be designed for optimizing both electronics and optics simultaneously. Since CMOS processes are optimized for electronics and not intended for implementing photonics, they have limited materials and structures available. In other words, the performance of transistors should be compromised to modify the process for adding photonics. Thus, usually monolithic silicon photonic platforms use old CMOS technologies such as $180nm$, where MOS devices are less sensitive to changes required for optics and transistor's performance is traded off to enable photonics.

2.2.2 Silicon Photonics in Zero-change SOI CMOS Process

In this work, we are using an unmodified $45nm$ SOI CMOS process as our monolithic platform for developing silicon photonics. This process is one of the fastest CMOS technologies demonstrated with 11 metal layers. Many high-performance electronics used this node previously to build processors such as Playstation 3 Cell processor, the WiiU Espresso processor, and the IBM Power 7 [14].

Figure 2.5 illustrates the cross-section of layers available in this process. Key enabler of photonic devices is the high-index sub- $100nm$ thick crystalline silicon layer, which is normally used as the body of transistors. In order to guarantee that optical wave can be confined inside the designed waveguides in this layer, we only need to remove silicon substrate. Substrate removal is done by a single post-processing step via XeD_2 etching machine [1]. After this step, we achieved $3dB/cm$ waveguide loss [15] that is low enough not to affect the performance of photonic device.

Another critical element of optical links is the grating couplers to interface with the fibers. We are using vertical grating couplers fabricated in the same crystalline silicon layer. In addition, we added another layer of grating in the poly-silicon on top of the silicon grating pattern to add asymmetry and consequently reduce the coupling loss [16]. Current designs lead to less than $3.5dB$ per coupler loss [17].

Ring-modulators have been demonstrated in this process by placing interleaved lateral

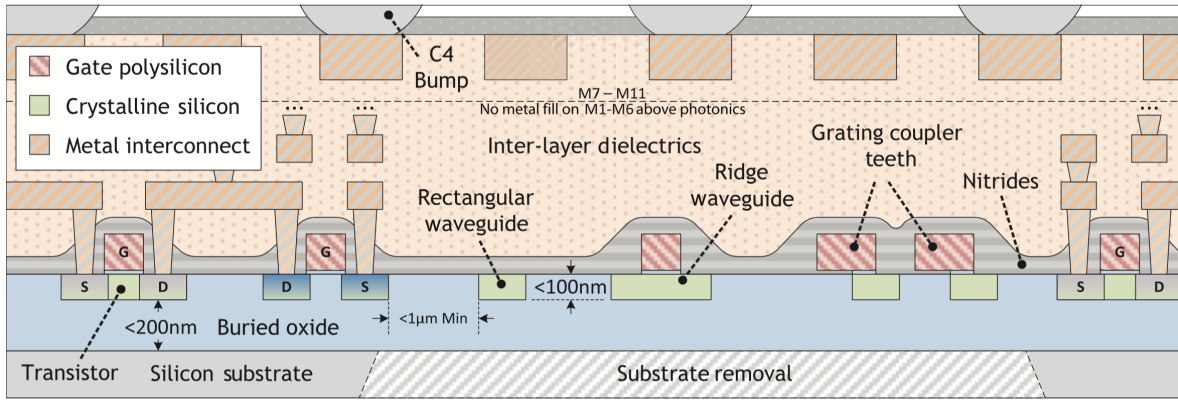


Figure 2.5: Cross-section of 45nm 12SOI CMOS process [9].

PN junctions along the looped around waveguide using existing doping levels for source/drain and well implants of transistors [18]. More details will be explained in Section 3.1.

Lastly, we have managed to implement photo-detectors using SiGe available in this process. This layer is normally used for stress-engineering of PMOS transistors in this process. Since Ge concentration is low, resonant detectors have been exploited to improve the responsivity up to $0.44A/W$ [19].

Chapter 3

Ring-resonator based Optical DAC

In this chapter, we propose the idea of building a purely optical DAC based on segmented ring-resonator design. First section elaborates on the details of ring-modulators in this process. Second section describes the methodology and benefits of this approach.

3.1 Spoked-ring Resonators

Active microring resonators have been implemented in this process using interleaved lateral PN junctions, giving rise to “spoked-ring” resonators/modulators [20]. The “spoked-ring” resonators used in this work has a cavity diameter of $10\mu m$ and is fabricated in crystalline silicon body layer (Figure 3.1).

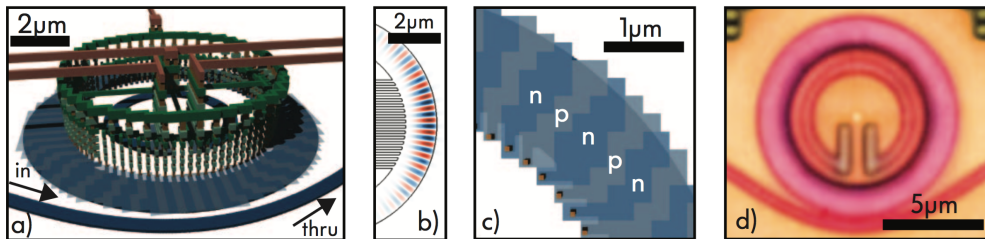


Figure 3.1: Spoked-ring modulator: (a) 3D rendering of layout; (b) FDTD simulation; (c) PN junctions mask; (d) Micrograph [20].

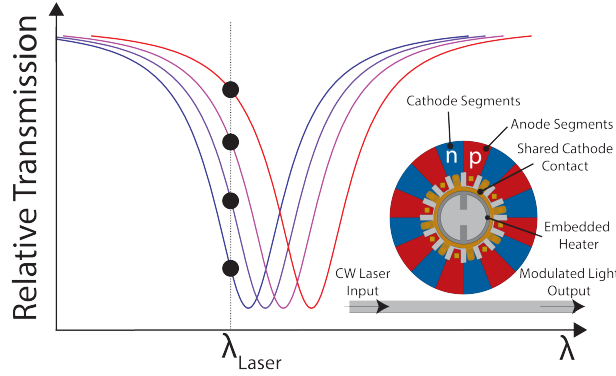


Figure 3.2: Optical DAC concept.

Although the ring width allows guidance of many transverse optical modes, bending the bus waveguide in the coupling region guarantees the single-mode operation by phase-matching and suppressing other modes. These rings can achieve higher than 10000 Q-factor with 3.2Thz FSR [20]. A resistive heater and weakly-coupled drop-port can be also added to the structures for closed-loop thermal tuning of the ring (Studied in Section 4.2). Moreover as shown in Figure 3.1, electrical contacts are placed far from the inner radius of the ring and connected together in a spoke shape in the center to avoid metallic optical loss. Conventionally, all P junctions are connected to each other making a single anode pin and similarly N junctions to form a unique cathode.

3.2 Optical DAC (ODAC)

Optical intensity DAC can be realized by separately driving each of “spoked-ring” anode segments and sharing all cathode segments of a spoked-ring modulator. Thus, the density of carriers in the cavity can be controlled by depleting a certain number of segments, consequently producing a corresponding resonance shift and an optical through-port intensity change (Figure 3.2).

In order to compare linearity of this approach versus the conventional method where the ring-resonator is driven by an electrical DAC, we will derive the transfer function of the ODAC. This transfer function can be obtained by substituting the resonance wavelength shift in the Lorentzian transfer function of the ring-resonators; Equation 3.1 shows the resonance

shift in wavelength, which is directly calculated from Equation 2.1. Also we know that Δn has a linear relation with electron/hole density ($\Delta N_{e/h}$) from [7] (Equation 3.2).

$$\Delta\lambda_0 = (L/m).\Delta n \quad (3.1)$$

$$\Delta n = k_e.\Delta N_e + k_h.\Delta N_h \quad (3.2)$$

Assuming an abrupt PN junction model for the segments, the total change in electron/hole density per cm^{-3} caused by active segments can be derived as follows:

$$x_e(V) = \frac{1}{N_D} \sqrt{\frac{2\epsilon_{Si}(V + V_b)}{q} \frac{N_A N_D}{N_A + N_D}} \quad (3.3)$$

$$\Delta N_e = \frac{M \times N_D \Delta x_e}{L} = \frac{M \times N_D}{L} \frac{x_e(0)}{\sqrt{V_b}} (\sqrt{V + V_b} - \sqrt{V_b}) \quad (3.4)$$

Equation 3.3 shows the depletion region width of a single PN-junction on the N-doped side, where the donor and acceptor doping concentrations are denoted by N_D and N_A , respectively. Total free electron density change is also expressed in Equation 3.4 by the summation over all the activated segments. Similarly, ΔN_h can be derived which is equal to ΔN_e since $N_D x_e = N_A x_h$ holds.

Finally, we can derive resonance wavelength shift as a function of M and $V + V_b$ from Equations 3.2 and 3.4, and substitute it in Equation 2.4 to rewrite the through-port intensity in terms of M and $V + V_b$ for any input wavelength (λ):

$$C = \frac{k_e + k_h}{m} \sqrt{\frac{2\epsilon_{Si}}{q} \frac{N_A N_D}{N_A + N_D}} \quad (3.5)$$

$$\lambda_{Shift}(M, V) = M(\sqrt{V + V_b} - \sqrt{V_b}) \times C \quad (3.6)$$

$$\alpha_{M,V}(\lambda) = 1 - \frac{A}{1 + 4\left(\frac{\lambda - \lambda_0 - \lambda_{Shift}(M,V)}{\Delta\lambda}\right)^2} \quad (3.7)$$

Figure 3.3 depicts the through-port relative intensity ($\alpha_{M,V}(\lambda)$) for different DAC codes (M) in the proposed optical DAC scheme in red and compares it against the conventional

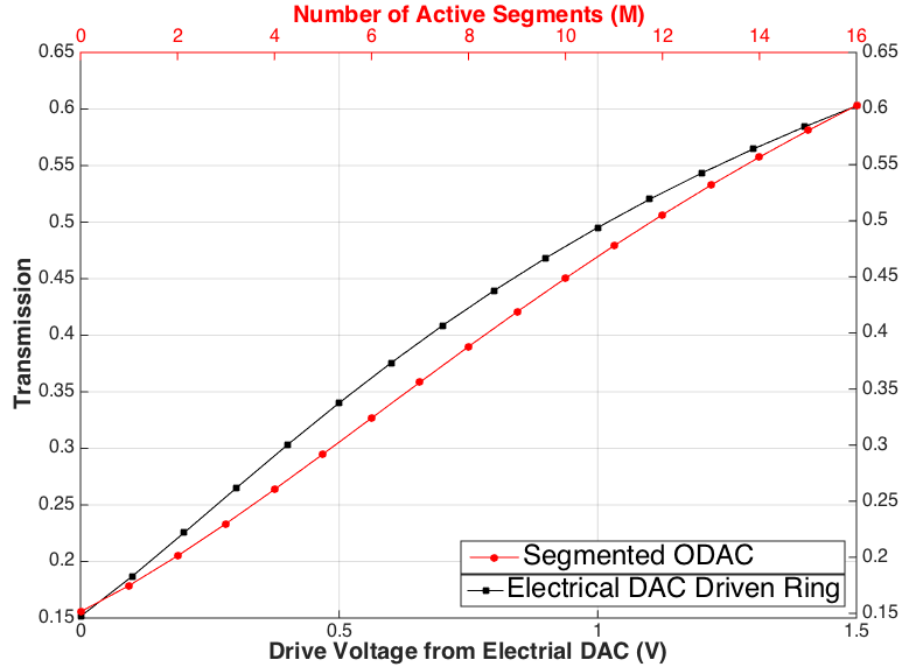


Figure 3.3: Linearity comparison of the proposed optical DAC vs. electrical DAC driven ring-resonator.

approach of electrical DAC driven ring-modulator (black curve) for the electrical DAC output voltages (V).

In this comparison, we assumed $1.5V$ voltage swing on 16 PN junction segments in a ring-resonator with Q-factor of $7.5K$, ER_i of $10dB$, and $50pm/V$ resonance shift. Intensity is measured at the wavelength that maximizes the ER for this ring (happens $20pm$ below $\lambda_0 = 1280nm$ in this case, where $ER = 6dB$).

Optical DAC showed improved linearity even under the assumption of ideal electrical DAC. Another advantage of this method for generating multi-level optical intensities is that by avoiding the use of electrical DAC, we can save area and energy and eliminate extra non-linearity. In addition, segmented ring optical DAC is less sensitive to process variation since structure is symmetric and has a small footprint.

Chapter 4

PAM4 Optical Transmitter

PAM4 modulation is a known solution to increase data-rates without requiring extra bandwidth. This scheme has recently become popular in electrical and optical link industries to alleviate high channel losses in electrical and modulator/PD bandwidth limitations in the optical domain. Different proposed approaches to build optical PAM4 transmitters are discussed in the first section. The rest of the sections elaborate on thermal tuning scheme and PLL which are critical sub-blocks of any ring-resonator based optical transmitter. Lastly, Section 4.4 discusses the complete transmitter design and its considerations.

4.1 Prior PAM4 Optical Transmitters

Optical PAM4 transmitters can be divided into two general categories; First, transmitters that use an electrical DAC to generate multi-level electrical signal which is fed into the modulator/laser such as MZI, ring-modulator, or even VCSEL lasers; Second category is realized by embedding sort of a DAC in the modulator structure and drive it digitally (or with an electrical DAC in a hybrid fashion). Two latest examples are shown in Figure 4.1.

First example from [3] is a MZI-based modulator with segmented phase-shifter arm. Although MZI's are considered to be more robust than ring modulator because they don't

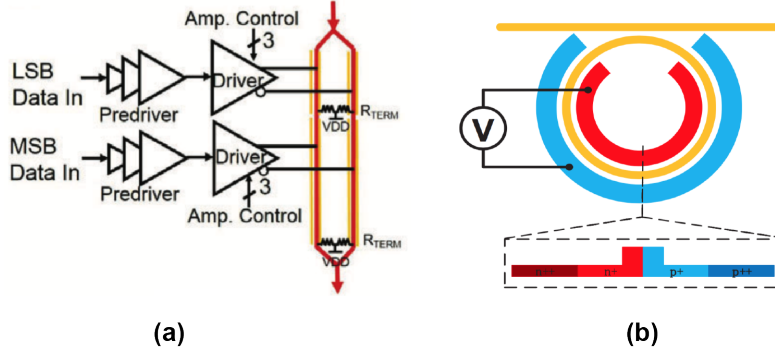


Figure 4.1: PAM4 optical transmitter architectures: (a) Segmented MZI with electrical DAC [3]; (b) Ring-modulator driven by an electrical DAC [21].

require thermal tuning, they have large footprints to achieve enough ER and that makes them area and energy inefficient and imposes RC bandwidth limitations. Authors in [21] replaced the MZI with a ring modulator and used an electrical DAC to linearize the ring behavior. We will demonstrate a electrical-DAC-less optical PAM4 transmitter in Section 3.2 and compare with these methods in Figure 6.1.

4.2 Ring-resonator Thermal Tuning

Most serious objection on using microring modulators is the resonance wavelength sensitivity to the temperature. Thermo-optical effects can be as high as $10GHz/K$ [22]; i.e. transmit eye can be totally closed by the temperature variation of couple degrees. This issue can be clarified by Figure 4.2. Dashed blue and red lines show the ring characteristic function corresponding with “0” and “1” data at the optimum locking position relative to the laser wavelength (λ_{Laser}) at T_0 temperature, where ER is maximized. Now if the temperature rises ($\Delta T > 0$) due to the circuits heating up or even optical power variations inside the ring, resonance wavelengths will be increased (“Red shift”), and the “0” and “1” optical levels will be closer to each other at the new temperature.

Our solution for this problem is published in [9], where a closed loop thermal tuning scheme is developed to continuously monitor the optical power level inside the ring and tune the ring temperature by using an embedded heater. By this scheme, we can optimize the

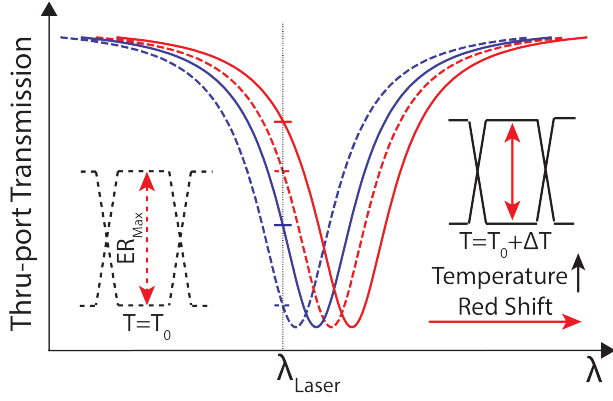


Figure 4.2: Thermal effects on ring-modulators.

eye-opening and keep the ring locked in terms of one of the symbol’s corresponding optical power. Moreover, this approach doesn’t require symbol-rate integrating front-ends and can be applied to any random data sequence (DC-balance is not required). In this work, we utilized this scheme for PAM4 signaling by modifying the controller digital backend.

4.3 High-Speed Digital PLL

Another sub-block of any high-speed transceiver is the clock source. Here, we designed a $20GHz$ LC-DCO based phase lock loop (PLL) and use dividers in order to feed $10GHz$ and $5GHz$ clocks to the transmitter serializers. Block diagram of this digital PLL (DPLL) is illustrated in Figure 4.3. DPLL is comprised of an LC-DCO, bang-band phase detector and a fully digital loop filter [23], which makes this design portable to any advanced CMOS technology node.

4.4 ODAC based PAM4 Transmitter

Finally we will demonstrate our PAM4 optical transmitter employing the ODAC idea from Section 3.2. Segmented ring-resonator in this design has 16 anode and cathode segments (can be extended to 64 segments). This segment partitioning leads to a 4-bit optical DAC,

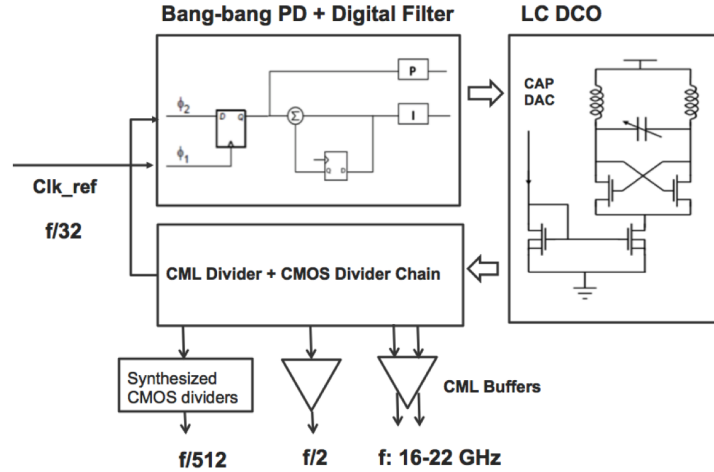


Figure 4.3: 20GHz Digital PLL block-digram.

because they are activated in a thermometer manner to achieve better linearity, electrical bandwidth and energy-efficiency, by minimizing the wire-to-wire capacitance parasitics of the segment control wires. Although PAM4 symbols consist of 2 bits, the extra 2 bits of DAC resolution enable linearization of the nonlinear Lorentzian through-port transfer characteristics of ring-resonators to transmit uniformly spaced PAM4 optical signal levels. The optical DAC resolution should be high-enough to be able to linearize the ring characteristics depending on the Q-factor of the resonator.

The CMOS transmitter is designed in a fully digital design flow with the capability of programming each symbol's corresponding optical amplitude level independently. Figure 4.4 shows the transmitter block diagram, where encoder translates 2-bit PAM4 symbols into 16-bit thermometer codes via a programmable look up table (LUT). Thermal tuning loop used here is a bit-statistical scheme described in Section 4.2. Micro-graphs of the test chip and major blocks are shown in Figure 4.5. The transmitter is operating in a double data rate (DDR) mode with a 10GHz clock generated from a DPLL from the previous section, which leads to a 20GS/s symbol-rate and 40Gb/s data rate PAM4 signal.

The complete electronics block, including a 16-slice modulator driver, encoder with LUT registers, PRBS and serializers, and thermal tuning control and its front-end circuits, occupies $200150\mu m^2$, which is approximately $3\times$ larger than the area occupied by the photonic devices (vertical couplers, waveguide, ring modulator and power monitoring photo-detector).

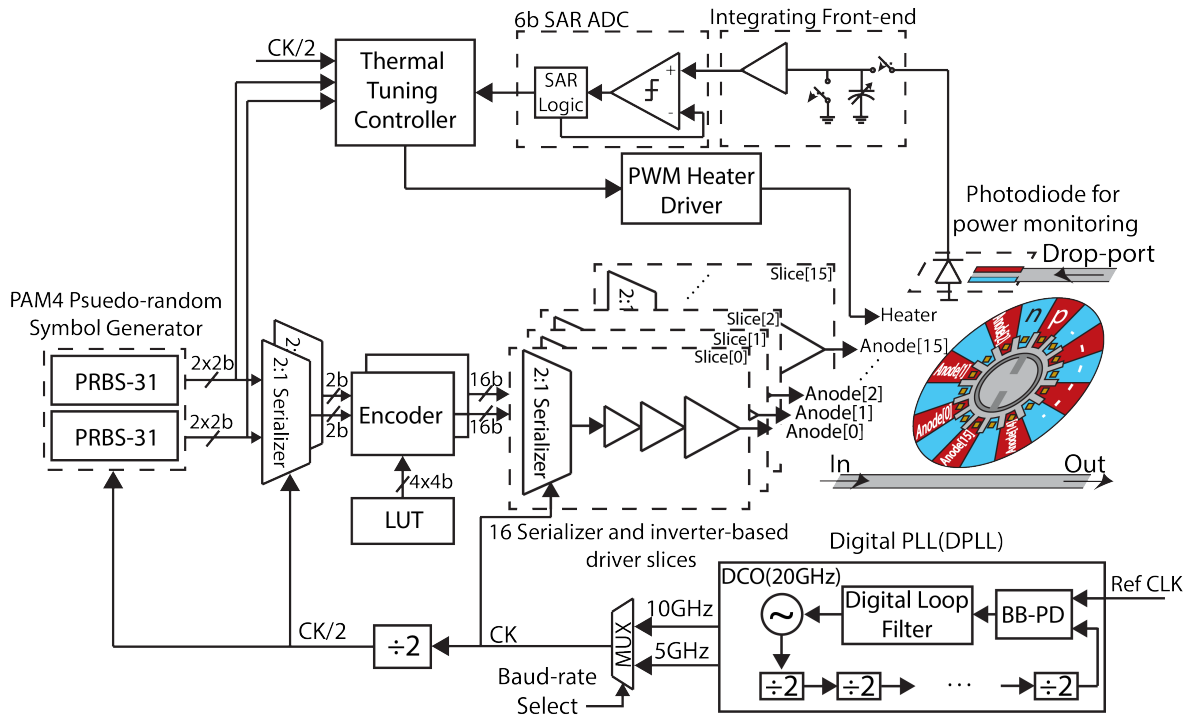


Figure 4.4: PAM4 transmitter block-diagram.

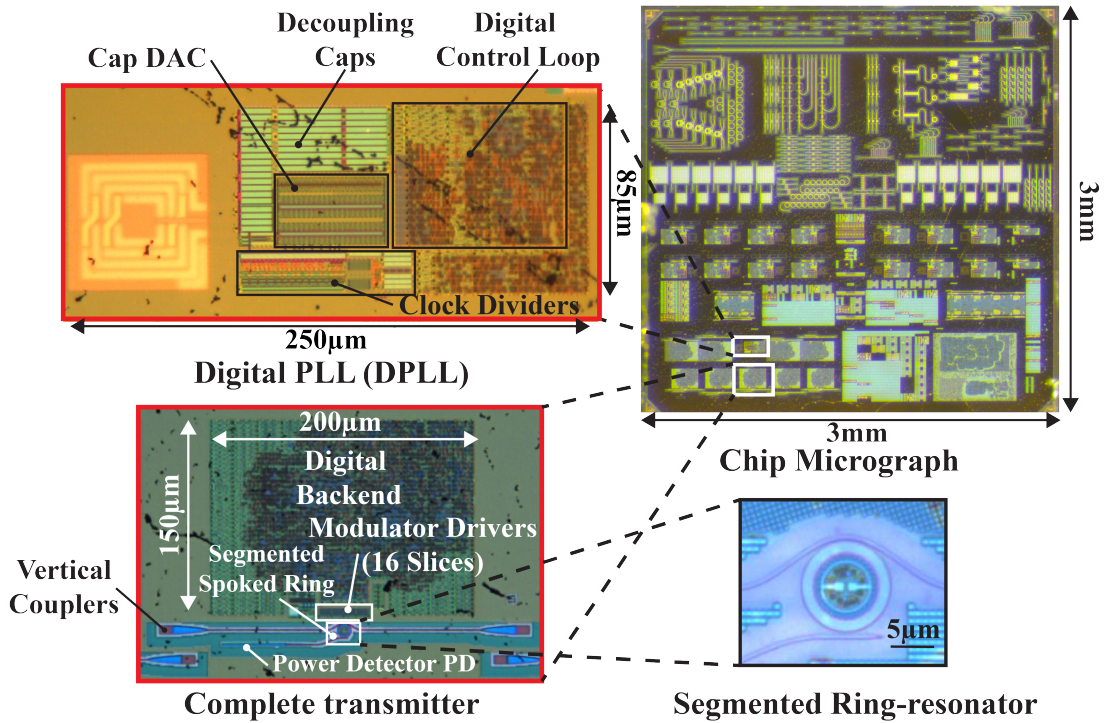


Figure 4.5: Chip micro-graphs.

Chapter 5

Measurement Results

The transmitter is designed and fabricated in a multi-project wafer run in the 45nm SOI CMOS technology with other electrical designs. The die is flip-chip assembled onto a PCB for electrical connectivity (Figure 5.1). This type of packaging is more common for high-performance electronics due to better power delivery, pin counts, and signal integrity of the I/O pins. The chip substrate was removed in a single post-processing step to prevent optical guided wave substrate radiation [1].

The test setup is shown in Figure 5.2; a tunable laser source couples into the backside of the chip via a lensed fiber and unidirectional vertical couplers in this platform with $3.5dB$ loss at $1280nm$ wavelength.

The transmitter is tested with the digital backend at nominal supply of $1V$ and modulator driver voltage at $1.55V$. The modulator is biased in depletion mode, and it sees a voltage swing of 0 to $-1.55V$. In order to examine the static functionality of the optical DAC, we swept the laser source wavelength with different DAC code settings at a low laser power of $-15dBm$ in order to avoid self-heating induced thermal drifts. The microring modulator achieved a FSR of $3.2THz$ and Q-factor of $7.5K$. The digital-to-optical relative power transfer function is measured and displayed in terms of output power versus the DAC code (Figure 5.3). Optimal mapping for balanced PAM4 eye-diagram is $(0, 3, 7, 15)$ in this example.

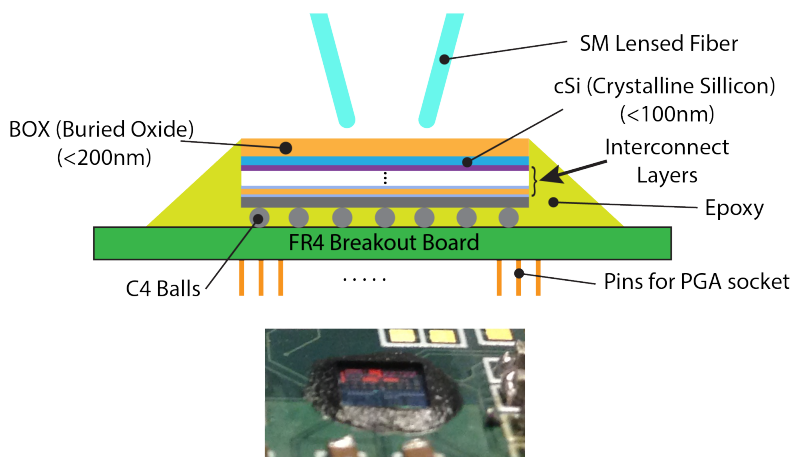


Figure 5.1: Flipchip packaging.

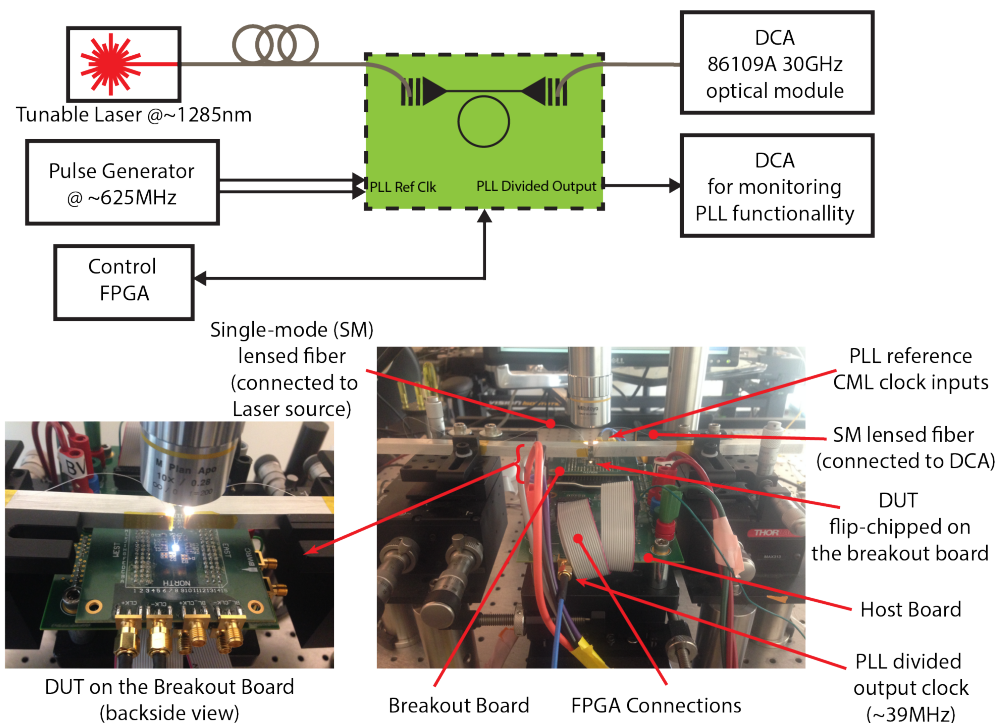


Figure 5.2: Test setup.

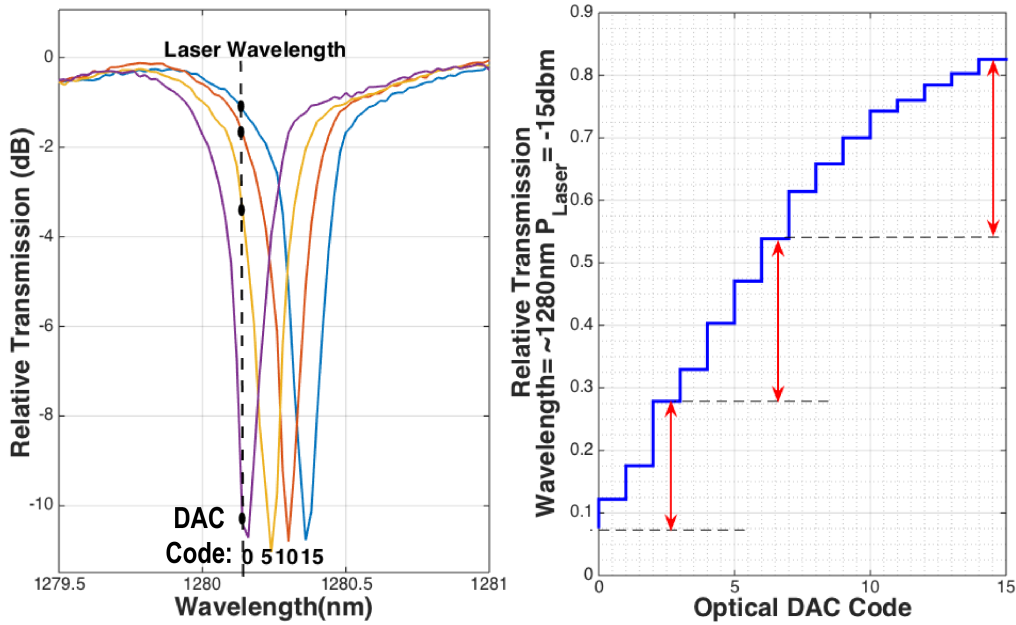


Figure 5.3: Static optical DAC measurements.

Next, we measured the high-speed dynamic characteristics of the transmitter. The measured rise/fall time is $\sim 20ps$ indicating that transmitter can potentially run faster than $20GS/s$. Figure 5.4 depicts the measured eye-diagrams captured by a $30GHz$ optical scope without any amplification in the optical path. The transmitted eye diagram is open with $3dB$ ER and $5.5dB$ IL at $\sim 1285nm$ laser wavelength. Notice, DAC codes should be adjusted for the new laser settings in this measurement and we realized (0, 5, 10, 15) is the optimal coding at this optical power in this case by sweeping all the codes.

The modulator and the driver achieved $20Gb/s$ NRZ with $155fJ/b$ and $40Gb/s$ PAM4

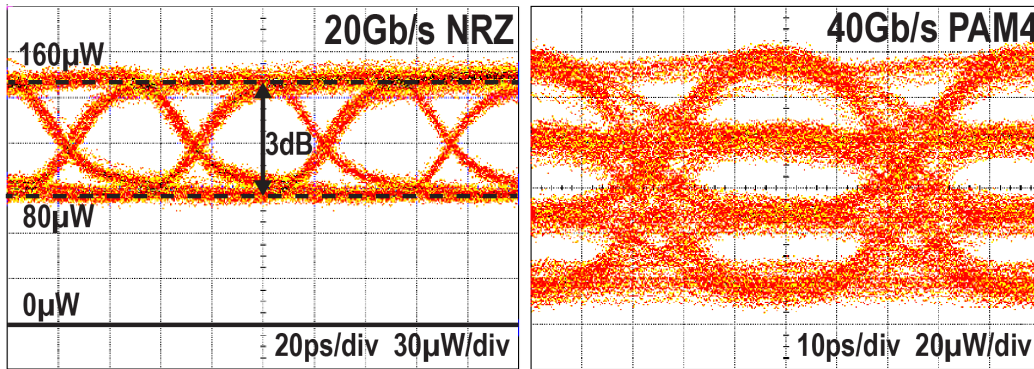


Figure 5.4: Transmit eye-diagrams.

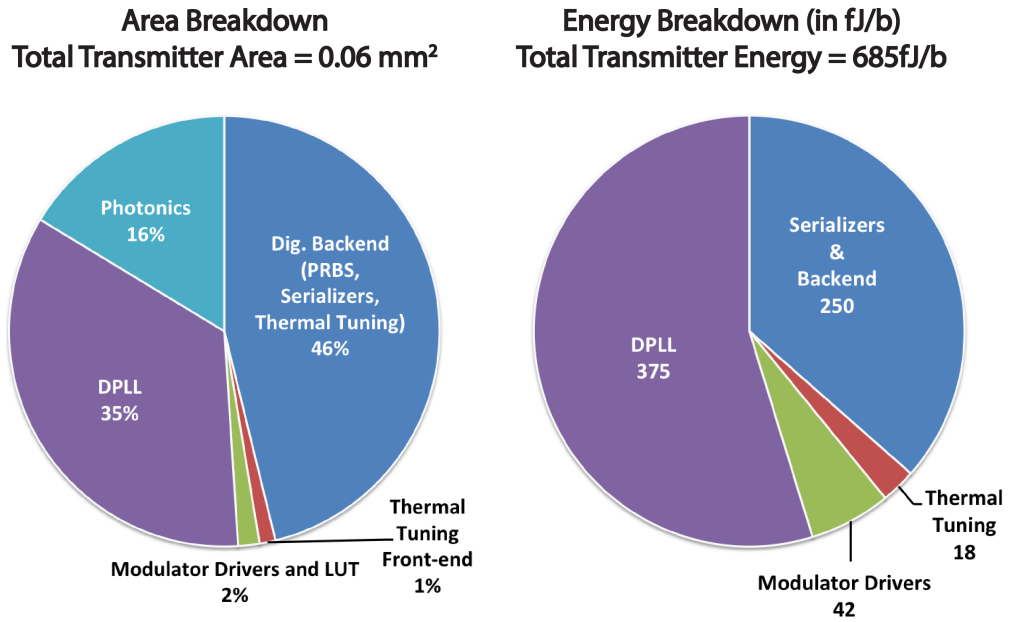


Figure 5.5: Transmitter area and energy breakdown.

with $42 fJ/b$ energy efficiency. The full transmitter energy efficiency is $685 fJ/b$ with the area of $0.06 mm^2$ including the PLL. Area/energy breakdown is summarized in Figure 5.5.

Chapter 6

Conclusion

Measured results are compared with other approaches in Figure 6.1. First two works [3, 2] are recent transmitters based on segmented MZIs and as explained in Section 4.1, they have poor energy-efficiency due to their large phase-shifter arms. Third transmitter [21] is a purely electrical DAC driven microring modulator method.

This work proves the benefits of avoiding electrical DAC, using microring modulators and advantage of monolithic silicon photonics platform. These elements helped us to improve both energy efficiency and bandwidth density over state-of-the-art PAM4 transmitters.

We have demonstrated a micro-ring resonator optical DAC and PAM4 transmitter implemented in a commercial 45nm SOI CMOS process. Leveraging the advanced process lithography this approach can scale the number of segments to support PAM8 and PAM16 modulations. In addition to high energy-efficiency, the complete transmitter occupies only $0.06mm^2$, assuming a dedicated PLL for each transmitter, achieving bandwidth density of $0.67Tb/s/mm^2$, which makes this approach suitable for systems-on-chip such as processors and switches with a large number of I/O links.

Reference	[CISCO, ISSCC 13]	[IBM, OI 15]	[Palermo, OI 16]	This Work
Integration	Hybrid	Monolithic	Hybrid	Monolithic
CMOS Technology	40nm	90nm	65nm	45nm
Driver Supply (V)	1	1.1	2.4	1.55
ER/IL (dB)	-	6.3/5	7/5	3/5.5
NRZ Data-rate (Gb/s)	20	25	-	20
NRZ Modulator and Driver Energy Efficiency (pJ/b)	4.5	-	-	0.155
PAM4 Data-rate (Gb/s)	20	56	40	40
PAM4 Modulator and Driver Energy Efficiency (pJ/b)	0.29	4.8	3.04	0.042
Photonics Area (mm ²)	0.18	1.5*	0.01*	0.01
Driver Area (mm ²)	0.2*	0.075*	0.07*	0.001+
Total Transmitter Area (mm ²)	-	-	0.08*	0.06**
Modulator and Driver BW Density (Tb/s/mm ²)	0.053	0.036	0.5	3.6
Transmitter BW Density (Tb/s/mm ²)	-	-	0.5	0.67**

* Estimated from figures

** Including full backend, thermal tuning blocks and DPLL

+ Including LUT area

Figure 6.1: Comparison and performance summary table.

Bibliography

- [1] C. Sun, M. T. Wade, Y. Lee, J. S. Orcutt, L. Alloatti, M. S. Georgas, A. S. Waterman, J. M. Shainline, R. R. Avizienis, S. Lin, B. R. Moss, R. Kumar, F. Pavanello, A. H. Atabaki, H. M. Cook, A. J. Ou, J. C. Leu, Y.-H. Chen, K. Asanović, R. J. Ram, M. Popović, and V. M. Stojanović, “Single-chip microprocessor that communicates directly using light,” *Nature*, vol. 528, no. 7583, pp. 534–538, 12 2015. [Online]. Available: <http://dx.doi.org/10.1038/nature16454>
- [2] X. Wu, B. Dama, P. Gothoskar, P. Metz, K. Shastri, S. Sunder, J. V. d. Spiegel, Y. Wang, M. Webster, and W. Wilson, “A 20gb/s nrz/pam-4 1v transmitter in 40nm cmos driving a si-photonics modulator in 0.13um cmos,” in *2013 IEEE International Solid-State Circuits Conference Digest of Technical Papers*, Feb 2013, pp. 128–129.
- [3] C. Xiong, D. Gill, J. Proesel, J. Orcutt, W. Haensch, and W. M. J. Green, “A monolithic 56 gb/s cmos integrated nanophotonic pam-4 transmitter,” in *2015 IEEE Optical Interconnects Conference (OI)*, April 2015, pp. 16–17.
- [4] M. Guarnieri, “The conquest of the atlantic [historical],” *IEEE Industrial Electronics Magazine*, vol. 8, no. 1, pp. 53–67, March 2014.
- [5] H. Liu, C. F. Lam, and C. Johnson, “Scaling optical interconnects in datacenter networks opportunities and challenges for wdm,” in *2010 18th IEEE Symposium on High Performance Interconnects*, 2010, pp. 113–116.
- [6] J. E. Heebner, V. Wong, A. Schweinsberg, R. W. Boyd, and D. J. Jackson, “Optical transmission characteristics of fiber ring resonators,” *IEEE Journal of Quantum Electronics*, vol. 40, no. 6, pp. 726–730, June 2004.

- [7] R. Soref and B. Bennett, "Electrooptical effects in silicon," *IEEE Journal of Quantum Electronics*, vol. 23, no. 1, pp. 123–129, Jan 1987.
- [8] C. Sun, "Silicon-photonics for vlsi systems," Ph.D. dissertation, Massachusetts Institute of Technology, 2015. [Online]. Available: <http://hdl.handle.net/1721.1/99784>
- [9] C. Sun, M. Wade, M. Georgas, S. Lin, L. Alloatti, B. Moss, R. Kumar, A. H. Atabaki, F. Pavanello, J. M. Shainline, J. S. Orcutt, R. J. Ram, M. Popovi, and V. Stojanovi, "A 45 nm cmos-soi monolithic photonics platform with bit-statistics-based resonant microring thermal tuning," *IEEE Journal of Solid-State Circuits*, vol. 51, no. 4, pp. 893–907, April 2016.
- [10] X. Zheng, S. Lin, Y. Luo, J. Yao, G. Li, S. S. Djordjevic, J. H. Lee, H. D. Thacker, I. Shubin, K. Raj, J. E. Cunningham, and A. V. Krishnamoorthy, "Efficient wdm laser sources towards terabyte/s silicon photonic interconnects," *Journal of Lightwave Technology*, vol. 31, no. 24, pp. 4142–4154, Dec 2013.
- [11] B. R. Koch, E. J. Norberg, B. Kim, J. Hutchinson, J.-H. Shin, G. Fish, and A. Fang, "Integrated silicon photonic laser sources for telecom and datacom," in *Optical Fiber Communication Conference/National Fiber Optic Engineers Conference 2013*. Optical Society of America, 2013, p. PDP5C.8. [Online]. Available: <http://www.osapublishing.org/abstract.cfm?URI=NFOEC-2013-PDP5C.8>
- [12] K. T. Settaluri, S. Lin, S. Moazeni, E. Timurdogan, C. Sun, M. Moresco, Z. Su, Y. H. Chen, G. Leake, D. LaTulipe, C. McDonough, J. Hebding, D. Coolbaugh, M. Watts, and V. Stojanovi, "Demonstration of an optical chip-to-chip link in a 3d integrated electronic-photonics platform," in *European Solid-State Circuits Conference (ESSCIRC), ESSCIRC 2015 - 41st*, Sept 2015, pp. 156–159.
- [13] F. Y. Liu, D. Patil, J. Lexau, P. Amberg, M. Dayringer, J. Gainsley, H. F. Moghadam, X. Zheng, J. E. Cunningham, A. V. Krishnamoorthy, E. Alon, and R. Ho, "10-gbps, 5.3-mw optical transmitter and receiver circuits in 40-nm cmos," *IEEE Journal of Solid-State Circuits*, vol. 47, no. 9, pp. 2049–2067, Sept 2012.
- [14] R. Kalla, B. Sinharoy, W. J. Starke, and M. Floyd, "Power7: Ibm's next-generation server processor," *IEEE Micro*, vol. 30, no. 2, pp. 7–15, March 2010.

- [15] J. S. Orcutt, B. Moss, C. Sun, J. Leu, M. Georgas, J. Shainline, E. Zraggen, H. Li, J. Sun, M. Weaver, S. Urošević, M. Popović, R. J. Ram, and V. Stojanović, “Open foundry platform for high-performance electronic-photonics integration,” *Opt. Express*, vol. 20, no. 11, pp. 12 222–12 232, May 2012. [Online]. Available: <http://www.opticsexpress.org/abstract.cfm?URI=oe-20-11-12222>
- [16] J. Notaros, F. Pavanello, M. T. Wade, C. Gentry, A. Atabaki, L. Alloatti, R. J. Ram, and M. Popovic, “Ultra-efficient cmos fiber-to-chip grating couplers,” in *Optical Fiber Communication Conference*. Optical Society of America, 2016, p. M2I.5. [Online]. Available: <http://www.osapublishing.org/abstract.cfm?URI=OFC-2016-M2I.5>
- [17] M. T. Wade, F. Pavanello, R. Kumar, C. M. Gentry, A. Atabaki, R. Ram, V. Stojanovi, and M. A. Popovi, “75couplers in a 45 nm microelectronics cmos process,” in *2015 IEEE Optical Interconnects Conference (OI)*, April 2015, pp. 46–47.
- [18] J. M. Shainline, J. S. Orcutt, M. T. Wade, K. Nammari, B. Moss, M. Georgas, C. Sun, R. J. Ram, V. Stojanović, and M. A. Popović, “Depletion-mode carrier-plasma optical modulator in zero-change advanced cmos,” *Opt. Lett.*, vol. 38, no. 15, pp. 2657–2659, Aug 2013. [Online]. Available: <http://ol.osa.org/abstract.cfm?URI=ol-38-15-2657>
- [19] L. Alloatti, D. Cheian, A. Atabaki, and R. J. Ram, “Zero-change cmos photodiode with 0.44 a/w responsivity,” in *Optical Fiber Communication Conference*. Optical Society of America, 2016, p. Tu2D.8. [Online]. Available: <http://www.osapublishing.org/abstract.cfm?URI=OFC-2016-Tu2D.8>
- [20] M. T. Wade, J. M. Shainline, J. S. Orcutt, C. Sun, R. Kumar, B. Moss, M. Georgas, R. J. Ram, V. Stojanovi, and M. A. Popovi, “Energy-efficient active photonics in a zero-change, state-of-the-art cmos process,” in *Optical Fiber Communications Conference and Exhibition (OFC), 2014*, March 2014, pp. 1–3.
- [21] A. Roshan-Zamir, B. Wang, S. Telaprolu, K. Yu, C. Li, M. A. Seyedi, M. Fiorentino, R. Beausoleil, and S. Palermo, “A 40 gb/s pam4 silicon microring resonator modulator transmitter in 65nm cmos,” in *2016 IEEE Optical Interconnects Conference (OI)*, May 2016, pp. 8–9.

- [22] G. Li, X. Zheng, J. Yao, H. Thacker, I. Shubin, Y. Luo, K. Raj, J. E. Cunningham, and A. V. Krishnamoorthy, “25gb/s 1v-driving cmos ring modulator with integrated thermal tuning,” *Opt. Express*, vol. 19, no. 21, pp. 20 435–20 443, Oct 2011. [Online]. Available: <http://www.opticsexpress.org/abstract.cfm?URI=oe-19-21-20435>
- [23] J. Crossley, E. Naviasky, and E. Alon, “An energy-efficient ring-oscillator digital pll,” in *Custom Integrated Circuits Conference (CICC), 2010 IEEE*, Sept 2010, pp. 1–4.